Charge Transfer and Photocurrent in Interfacial Junctions between Bismuth and Graphene

Tito E. Huber, Scott D. Johnson, John H. Belk, Jeff H. Hunt, and Khosro Shirvani

Phys. Rev. Applied **10**, 044020 — Published 8 October 2018

DOI: 10.1103/PhysRevApplied.10.044020

Charge Transfer and Photocurrent in Interface Junctions between Bismuth and Graphene

Tito E. Huber,[1,*)] Scott. D. Johnson,[1] John H. Belk,[3] Jeff H. Hunt[4] and Khosro Shirvani[5].

[1]Howard University, 500 College St. NW, Washington, DC 20059. USA

[3] The University of Missouri, MO 63134, USA

[4] The Boeing Company. 900 N Sepulveda Blvd, El Segundo, CA 90245. USA

[5]Rowan University, 201 Mullica Hill Rd, Glassboro, NJ 08028

Abstract

Graphene, the two dimensional monolayer of carbon, is an essential building block for advanced electronic applications. Graphene is often integrated with bulk conductors, metals and semiconductors, for optoelectronic applications. The semimetal bismuth, that shares many electronic properties with these other conductors, is interesting because like graphene, it is a gapless conductor of high electronic mobility with linear dispersion relations and low electronic density. We studied the doping of graphene by Bi and the interfacial electric dipole. Graphene Raman spectroscopy results show that there is a very large charge transfer between graphene and bismuth. This doping is larger than in the interfaces of graphene with metals such as Cu and semiconductors such as Si. Our findings are in good agreement with recent theoretical results for graphene bismuth interfaces. We also present a demonstration of zero-bias photocurrent generation that is enabled by the electric dipole at the graphene bismuth interface.

*) thuber@howard.edu

I. INTRODUCTION

Graphene, the novel two-dimensional (2D) material consisting of a single monolayer of carbon, has drawn strong interest due to its extraordinary electronic and optical properties [1]. Because of its high electronic mobility [2] and strong doping effects [3,4], graphene has attracted intense interest in the field of optoelectronic devices [5]. Photodetectors based on single-layer graphene (SLG) between metal contacts demonstrate fast response [6-8] and feature broad detecting spectral widths related to the gapless nature of its conduction band even if the missing bandgap inevitably leads to a low on-off ratio as opposed to 2D-semiconductors [9-13].

Photothermoelectric and photovoltaic effects are involved [14,15] in the photoresponse. SLG has limited absorption (2 %), inhibiting efficient photo carrier separation and accumulation and various schemes for increasing photoresponse have been proposed [16-21]. A special topic is the hybridization of graphene in the contact with semiconductors [20,21]. Compared to semiconductors, bismuth has new interesting properties. Like graphene, bismuth is gapless. Bulk Bi Fermi surface features small electron pockets centered at the three L points of the Brillouin zone and also a hole pocket at the T point. Bi electron n and hole p density ($n = p$) of 10^{18} cm^{-3} is low, more comparable to those found in lightly doped semiconductors than those of metals, where the density is ~ 10^{23} cm^{-3}. The bulk electronic mobility is high, exceeding 10^4 $cm^2V^{-1}cm^{-1}$at room temperature [22]. This is comparable to the electron mobility of a metal such as silver. Spin-orbit surface states that can dominate transport in Bi nanostructures, also display exceptionally high mobilities [23]. In spite of these prospects, the optoelectronic properties of the interface between bismuth and graphene have received little attention.

When a conductor makes direct contact to graphene, the difference in work functions lead to electron transfer in order to equilibrate the Fermi levels resulting in the formation of a dipole

layer and an associated potential step at the interface. Such energy barriers have been demonstrated for graphene metal (copper) junctions [6,24,25] and for graphene semiconductor interfaces [26] but have not been studied in bismuth graphene interfaces. Also, the graphene bismuth interface can be expected to be more complex than the one between graphene and metal due to the spatial response of the electron gas to the barrier as the Thomas-Fermi screening length Λ of Bi is exceptionally long, approximately 4 nm [27] because the its low density of states. In contrast, Λ is only a fraction of a nanometer for metals and heavily doped semiconductors [28]. With regard to Λ , Bi appears to be similar to lightly doped semiconductors, that also feature a long Λ. However, graphene junctions with lightly doped semiconductors feature a Schottky barrier, that is rectifying [28,29]. This special combination of interfacial electronic properties of bismuth motivated us to study the photoresponse of a bismuth graphene interface in order to gain insight into the role of screening length, Schottky barrier phenomena and internal electric fields in Bi graphene interface.

Bismuth is employed in several novel photodetector designs [30,31] since it has a broad absorption band [32-34] with a threshold at ~ 1000 cm^{-1} [32-34] that is a pathway for electron-hole (e-h) pair generation. See Supplemental Material [35] for details. Yao et al [30] observed a photocurrent in bismuth films and his interpretation is that the e-h pairs, under bias, produce a current. The phenomenon that we wanted to explore is the zero-bias current driven by internal fields at the bismuth metal contact. In the case of our graphene hybrids, the internal field is associated with the work functions of bismuth and graphene and the energy barriers in the contact [3,36]. Guided by this work, we considered that the modifications of SLG that are observed via Raman can be associated with energy barriers and graphene doping [37-39]. We will also discuss graphene hot carriers [14,15,40] and thermoelectric response [41,42].

II. METHODS

We employed hybrid heterostructures composed of 200-nm Bi nanowire arrays which are capped with SLG. The arrays of 200-nm were fabricated employing the technique of pressure injection [43-45] of templates with molten Bi, a method that has been successfully employed

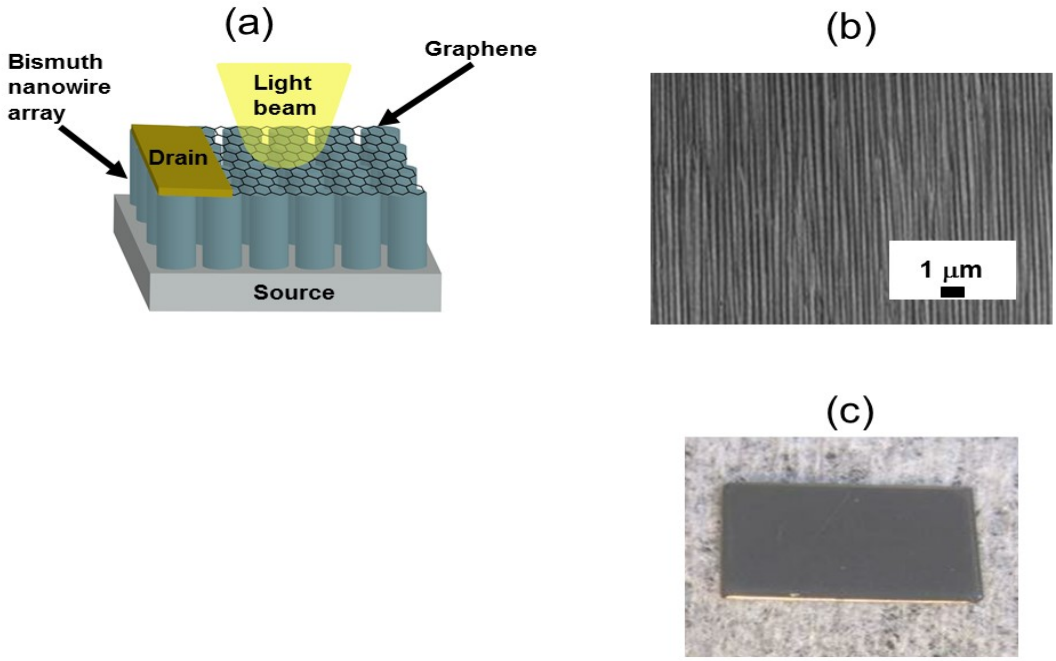

Figure 1: Bi Nanowire Array Array Device Structure. (a) Schematic design of the photodetector device. The I(V) between the bulk bismuth base and the drain is linear and the resistance is 90 Ohms. (b) SEM image of the nanowire array. (c) Optical microscope image of the nanowire array showing that the nanowire array appears dark.

with 100-μm thick alumina templates and pore diameters in the range of 20 to 200 nm. The alumina template used in this work was sold commercially under the trade name Anopore (Whatman, MA, USA) and was made by the anodization of aluminum. The template is a 55 microns thick plate of alumina which supports an array of parallel cylindrical channels running perpendicular to the plate. An illustration of the nanowire array fabrication process is presented

in the Supplemental Material [35]. The alumina plates and the bismuth were packed in a thin glass tube. The tube was closed at the bottom. The tube was then inserted into the reactor of a high temperature/high pressure injection apparatus. The molten bismuth was injected in the channels of the alumina template. Pressure was needed to overcome the effect of the surface tension combined with the non-wetting characteristics of bismuth on the template walls. A reactor and pump rated for 10 kBar service were employed. The reactor temperature is 300 C. When the injection was complete, the melt solidified inside the alumina channels. X–ray diffraction shows that the crystal grains were larger than the wire diameter and were oriented with the crystalline c-axis along the wire length. The single layer graphene film (SLG) was fabricated by chemical vapor deposition (CVD) on copper, detached and transferred on our nanowire array by Graphenea, Cambridge, MA, USA. The nanowire array samples are polished mechanically after cleaving prior to the graphene transfer. Therefore graphene rests on a smooth surface. The electrode indicated as drain is a drop of E4110-PFC silver epoxy (Epoxy Technology, Billerica, MA, USA). After curing at 120 C, the drop is essentially a solid of sintered silver nanoparticles [43]. It was observed that this solid adheres strongly to the graphene. In addition, samples of SLGs on (111) Bi single crystal surfaces were fabricated and measured. The sample, which is 1mm thick and has a cross-section of 0.5 cm^2, was prepared by cleaving a slab section from a single crystal. For comparison purposes, we also measured SLG samples on polycrystalline silicon. This sample was purchased from ACS, Medford, MA, USA. We also tested a sample of SLG on silicon dioxide (Graphenea, MA, USA). Raman spectra were collected at room temperature with the Ranishaw InVia spectrometer. The laser wavelength is 514.5 nm and the laser power is 0.5 mW. The area of the laser spot in smaller than 1 μm^2 and the spectral resolution is better that 1 cm^{-1}.

III. RESULTS AND DISCUSSION

The graphene photodetector device based on the 200-nm Bi nanowire arrays (NWA) is illustrated in Figure 1a. NWA magnetotransport at low temperature has been characterized previously [44,45] and it was found that such nanowires have a semimetallic interior with surface states on the periphery where, at room temperature, the semimetal dominates the electronic properties. An scanning electron microscope (SEM) image of the NWA is shown in Figure 1b. The sample is 1.5 mm × 2 mm. Its I-V measured between the drain and the source, is linear at room temperature and its resistance is 90 Ohms. There is no evidence of rectifying behavior that would point to a Schottky barrier. Fig 1c is an optical image of the interface. The surface appears black because of light trapping. Light trapping entails broadband optical absorption by nanowires oriented in the optical incident direction. Light trapping is well known and can be traced to the optical properties of individual nanowires [46-57]. Array geometry, nanowire shape, and order have previously been shown, both experimentally and theoretically, to control the spectral position and breadth of the absorbing region. There are few studies that extract the penetration of the optical fields in the nanostructure. In our sample, the light penetrates at least a wavelength (~500 nm). This was revealed by our experiments with visible light where we observe that the reflected light is polarized when the direction of incidence is off-normal. Our observation of polarization distinguishes the absorption in our samples from the plain broadband absorption that is caused by an absorbing coating. This property suggests that the nanowire array optical properties are those of metamaterials as presented by Yao *et al*. [55]. Our nanowire array device overcomes the major obstacles for the realization of a graphene/bismuth hybrid for optical detectors, namely, poor optical absorption by graphene and

the high reflectivity of bismuth. In the configuration that we employed, light trapping coexists with the high conductance path for the photocurrent. Light trapping has been exploited in photovoltaics and light harvesting [58,59].

In Figure 2, we show Raman spectra of a samples in the range from 700 to 3400 cm^{-1}. Our observations compared favorably with the observations by Li *et al*. [60] and Tongay *et al*.

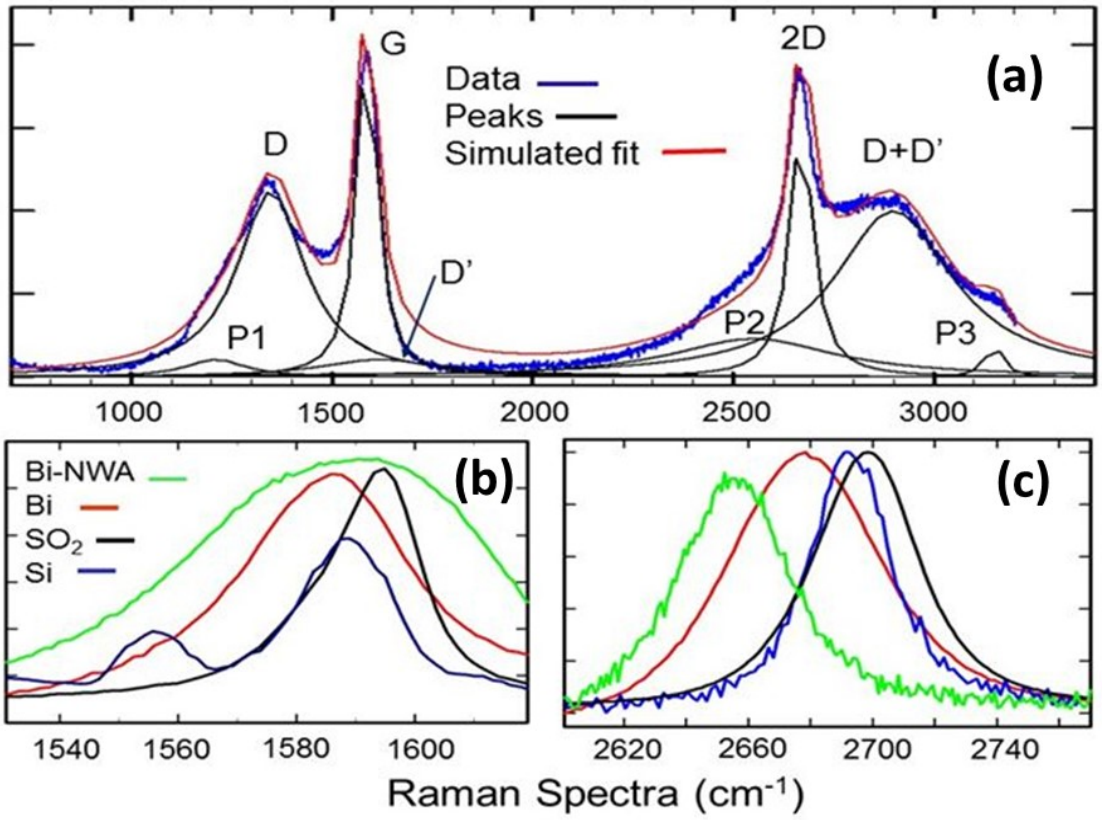

Figure 2: (a) Raman spectra of CVD-grown graphene after transfer onto Bi-nanowire arrays (NWA). The blue curve is the raw data, where the smooth background has been subtracted. The black curve show the individual peaks in the spectra as indicated in the legend and the red curve shows the simulated fit. See Table I in the Supplemental Material [35], for peak positions, intensities and full width at half-maximum (FWHM). (b) The Raman-spectra G-peak. The black curve is the measurement on graphene/SiO2 and the other curves are for graphene/substrate combinations as indicated in the legend. (c) Same as in (b) for the Raman-spectra 2D peak.

[61]. The four characteristic peaks for graphene at 1590 cm^{-1} (G-band), 1350 cm^{-1} (disorder D-band), 2670 cm^{-1} (2D band) and 2900 cm^{-1} (D+D') are observed indicating the unique electronic structure of graphene is preserved. The defect D' line at 1600 cm^{-1} is also observable. In addition

we observe three lines that have not being identified before, namely 1210 cm^{-1} (P1), 2450 cm^{-1} (P2) and 3150 cm^{-1} (P3). The various peaks are fit with Lorentzian functions and the peaks position, amplitudes and full width at half maximum (FWHM) are presented in Table I of the Supplemental Material [35]. The D and D' peaks evidence disorder. Additionally, the width of the D line that is more than twice that of the G and 2D lines which also indicates disorder. The disorder that is observed can be characterized following Cançado *et al*. [37]; they presented a systematic study of the ratio between the integrated intensities of the D and G Raman lines of nanographite with different crystalline sizes. Accordingly, we estimate the crystalline size of our samples to be 20 nm. The SLG disorder that was observed by us can be characterized also using the method of comparison with ion-damaged graphene [38,39]. Considering that the breath of the D peak is twice that of the G peak, the I_D/I_G ratio of 1.14 is the same that is observed in ion-damaged samples with the mean distance between damage centers L_D of 8 nm. However, we believe that both estimates of 20 nm and 8 nm are overestimates. The reason is that the D line is "locally activated", i.e., it only becomes "active" in the near vicinity of an imperfection (such as an edge or a point defect or as in our case by contact). Experimental and theoretical studies show that an activated area has an I_D/I_G ratio of roughly 4.2 [39]. We assume that the areas of graphene that are not contacted do not contribute to the D line. Since the SEM shows that the fractional area occupied by Bi nanowires is 30 % this simple model of "locally activated" areas predicts $I_D/I_G \sim 1.2$, which is very close to our experimental value of 1.14. In the low wavenumber range (10-500 cm^{-1}), there were peaks at 70 and 100 cm^{-1} which were consistent with the Eg and Ag vibrational modes of bulk Bi [62].

Raman can be employed to characterize doping in graphene and to evaluate the charge density. The 2D and G lines that are shown, expanded, in Figure 2b and 2c, are interesting. In

comparison to the Raman peaks of graphene on silica, the center frequencies of the G and 2D peaks are shifted by various amounts. When SLG is in contact with the substrate, equilibration of the Fermi level throughout the system gives rise to a charge transfer between the graphene and the substrate, thereby creating an electrical dipole. The G and 2D bands are both strongly influenced by the carrier concentration and they have been extensively studied for doping characterization [4,39]. These experiments were carried out in undamaged SLG and doping was performed in an electrochemical manner. It was found that the position of the 2D band depends on the Fermi energy E_F. The 2D band position changes as the Fermi energy shifts. Neglecting the graphene damage in our samples, our observation of large 2D line Raman shifts of $-(20 \pm 5)$ cm^{-1} and $-(45 \pm 5)$ cm^{-1} for the Bi and Bi nanowire arrays samples, respectively, can be accounted for by an electron doping amounting to $Q = (-2 \pm 0.5)\ e \times 10^{13}$ cm^{-2} for Bi and $Q = (-4 \pm 0.5)\ e \times 10^{13}$ cm^{-2} for Bi nanowires. Here e is the electron charge. The large value of Q for Bi nanowires in comparison to the Bi crystal sample is assigned to curvature induced electric field enhancements (lighting-rod effect) as observed in graphene near sharp metal contacts by Echtermeyer et al. [14]. The 2D Raman shifts that are observed in bismuth graphene contacts is larger than in the case of graphene in contact with the other metals and semiconductors that we have investigated. This condition is illustrated in Figure 2.c. for silicon. Such high level of doping explains the observation of a reduced intensity of the 2D line, I_{2D}, with respect to the intensity of the G line, I_G. The ratio I_{2D}/I_G can be as large as 3.5 for undoped graphene whereas for graphene in contact with bismuth nanowires the ratio of intensities I_{2D}/I_G is only 0.75.

Giovanetti *et al.* [3] and Khomyakov *et al*. [36] studied the adsorption of graphene on metal substrates using DFT calculations. It was shown that the bonding of graphene to some metals, notably Cu, is so weak that the unique graphene electronic structure is preserved. The

interaction lead to charge transfer and doping that shifts the Fermi level with respect to the conical points. Their study provides an insight into our observations. They showed that the difference of work functions of the substrate and SLG is the most relevant parameter that controls graphene doping. A review of the literature shows that the work function of bismuth W_{Bi} is between 4.2 and 4.3 eV [63]. The work function of suspended graphene W_G is between 4.9 and 5.2 eV [64,65]. Accordingly, because the work function of bismuth is lower than that of SLG, doping should be is n-type, as observed. The bismuth-graphene work function difference ($W_{Bi} - W_G$) ~ −0.7 eV. This work function difference is larger than for any of the metals (Al, Ag, Cu, Au, Pt) that were analyzed. For example, the element with the lowest work function that was analyzed, Al, has a work function difference of −0.25 eV and in this case the calculated graphene Fermi energy is between −0.1 eV and −0.6 eV whereas, based on the Raman data, our estimate of the Fermi energy is -0.8 eV. Since a large bismuth-graphene work function difference causes a large doping, this explains the large doping that we found for graphene Bi interfaces in our Raman spectroscopy experiments.

Current understanding of the interface dipole in our case is preliminary. Figure 3 is a schematic (not to scale) energy diagram of the interface. This diagram is adapted from the one for metals [3,36]. Work functions W_{Bi} of bismuth and W_G of graphene are represented. Also, the Fermi energy E_F of the electrons (metal and graphene) is represented. ΔE_F ($\Delta E_F < 0$ because SLG is n-doped) is the difference of the graphene Fermi energy with respect to the Dirac point. We have estimated, on the basis of Raman spectroscopy results, that $\Delta E_F \sim -0.8$ eV.

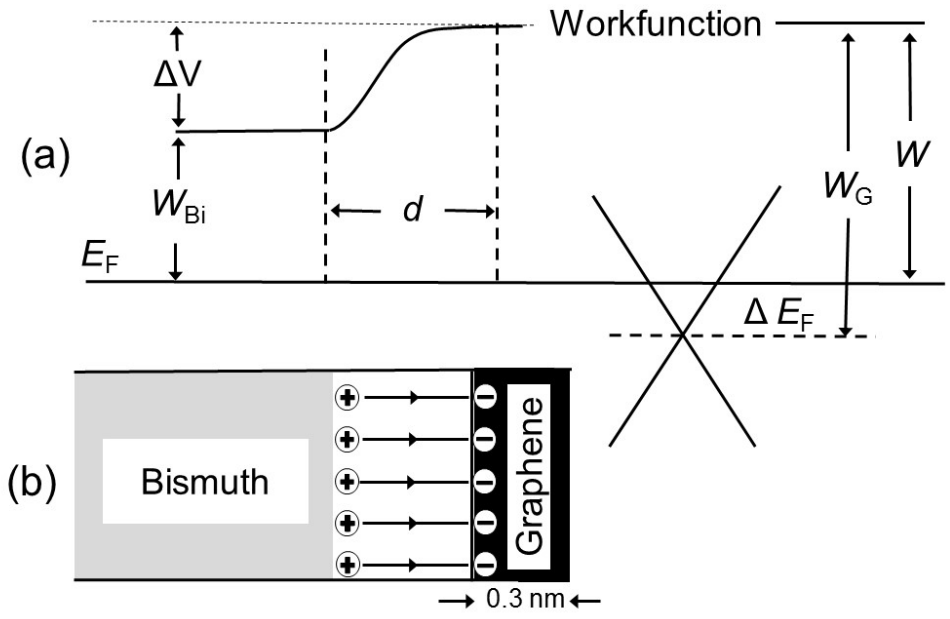

Figure 3: (a). Schematic view of the band profile and dipole formation at the semimetal-graphene interface. Work functions W_{Bi} of bismuth, W_G of graphene and the actual work function of graphene W are shown. The Fermi energy E_F of the electrons in graphene is represented also. The dashed line indicates the Fermi level of graphene at the neutrality point where ΔE_F is ~ −0.8 eV. The distance required to equilibrate the workfunction is d. (b). Physical diagram. We illustrate the interface dipole produced over the contact and the resultant electric field.

We illustrate the interface dipole, the potential step formation, where ΔV is the voltage drop produced over the contact, and the electric field due to the dipole. The work function of the graphene in contact with bismuth is $W = W_G + \Delta E_F$. In contrast to the high work function of suspended graphene of 4.9–5.2 eV, the work function of graphene under a metal electrode varies depending on the metal species. Our measurements indicate that, in the case of graphene in contact with bismuth, the work function is 4.2 eV. Therefore, our estimate of the barrier height $\Delta V = -0.1$ eV. Still, when applied to bismuth-graphene, the DFT approach may lead to an erroneous underestimate of ΔE_F unless the physics of the interfacial dipole considers the long Λ.

A number of theoretical and experimental studies of the graphene bismuth have been presented. Akturk *et al* [66] has studied the doping of graphene by bismuth atoms using density

functional theory (DFT) and found that Bi is weakly physisorbed, corroborating our observations. Clearly, there are important differences between the bulk Bi and single atoms on graphene. Moreover, Akturk *et al*. report charge transfer Q from the Bi atom to graphene in the range between 1.5 and 5 electrons per atom. Since the inter-bismuth distance is given as 0.3 nm, assuming a single-particle case, we can estimate the doping predicted by Akturk *et al*. to a full coverage case to range between 1.5×10^{14} and 5×10^{14} cm^{-2} . This compares favorably, within order of magnitude, with our experimental results for Bi and Bi nanowires. Although DFT predicts results slightly larger than in the experiment, it is clear that DFT provides a compelling physical picture of our electronic system. Chen *et al.* [67] have studied adsorption of Bi atoms and clusters on graphene grown by epitaxy (MEG). They observed a characteristic peak, corresponding to the p-band of Bi, in the tunneling spectrum and upon Bi deposition, electron transfer from MEG to Bi ad-atom.

Bismuth graphene photoelectric physics is relevant in our device and in several other novel photodetector designs [30,31] where the observation of broadband photoconductivity of bismuth films under ultraviolet to near infrared (1550 nm) light was reported. The observations were interpreted in terms of electron-hole (e-h) pairs. Pairs in the bulk of the film would normally recombine in a short time. However, with bias, an electrical current is established. The phenomenon that we explored with graphene-bismuth interfaces is the zero-bias current, presumably formed of e-h pairs, driven by the graphene bismuth internal fields. We focused on zero-bias current because this is key for light harvesting applications and because it gives us a handle on the interface dipole. The response in the UV, visible range and near-infrared is shown in Figure 4. We employed equipment consisting of a xenon lamp, monochromatic light sources consisting of LEDs, and light chopper. The equipment has been reported previously [41]. The

graphene heterostructure (Fig. 4), demonstrates broadband photoresponse from ultraviolet (UV) to the near infrared (NIR) range. The peak current that is observed at about 580 nm may originate from the relatively high power of the light source at this particular wavelength (the Xenon arc lamp). In the graphene bismuth samples, the photocurrent increases with decreasing chopping frequency and the trend that is uniformly observed for all the wavenumbers is PC $\sim f^{-\alpha}$, where $\alpha = (0.9 \pm 0.2)$. We observed this power-law frequency dependence of the photoresponse over three order of magnitude of excitation frequency consistent with a wide distribution of diffusion times. In contrast, in the case of devices based on Bi nanowire arrays capped with indium tin oxide, the zero-bias photoresponse current is much smaller and increases with chopping frequency f as PC $\sim f^{1/2}$. This square-root response indicates that the signal can be completely described by thermoelectric effects considering cooling rates given by heat diffusion

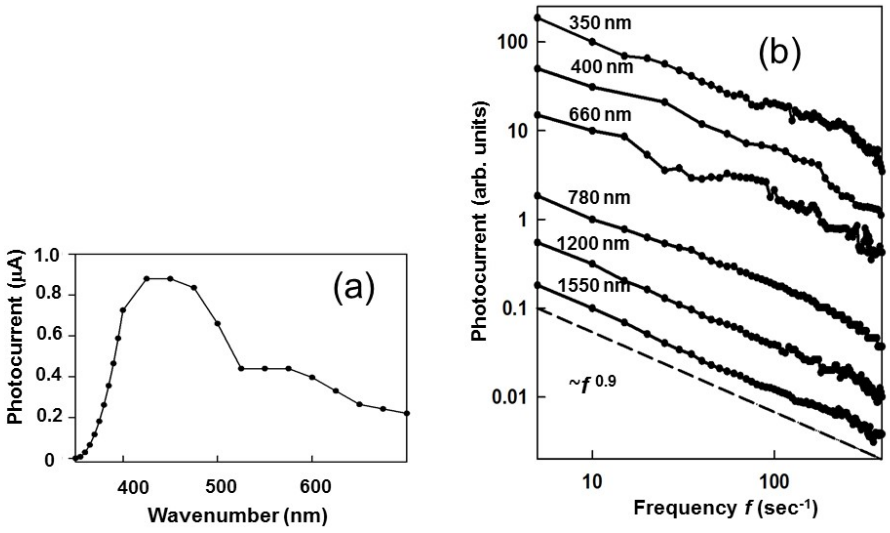

Figure 4. (a) Photocurrent (PC) of the heterostructure device as a function of the photoexcitation wavelength (from 300 nm to 700 nm). The photocurrent is measured between the bulk bismuth base and the drain (Figure 1) that is in contact with the graphene. (b) PC versus chopping frequency f for various wavenumbers. The various curves have been displaced vertically by arbitrary amounts. The dashed line shows the fit of a power-law dependence of the PC with an exponent of 0.9.

[41]. The wide distribution of response times in Bi-NWA-graphene is intriguing. A very

interesting model of transport was proposed by Nokidov *et al*. [68] to explain power-law current transients observed in partially ordered arrays of semiconducting nanocrystals. The model describes electron transport by a stationary Lévy process of transmission events and thereby requires no time dependence of system properties. Regardless of the specific model, the observation of an overall long photoresponse time (one second) indicate that the pair recombination processes in our sample are slow, many orders of magnitude slower than in bulk bismuth where is the recombination time is observed to be 10-20 ps [69].

The Bi/graphene interface is the subject of intense current research [70,71]. Recently, L. Jin *et al.* [71] studied a Bi nanowires/graphene heterostructure that features wrinkles in the graphene and reports giant optical absorption and in-graphene current generation. We believe that our internal field mechanism may contribute, additionally to the wrinkled surface that causes SLG to be gapped, to explain Jin's observation of an enhanced photoresponse.

Studies of photocurrent imaging in a graphene transistor show that the impact of the metal junctions extend only a few microns laterally in the graphene [6,24,25] Preliminary results lead us to believe that this applies to our Bi device also and that the area of the nanowire array that contributes to a photocurrent is the periphery of silver contact (drain in Figure 1). Future experiments should explore the operation of a device with two electrodes attached to the graphene cap so that we can measure the photocurrent with bias.

IV. CONCLUSION

In summary we have investigated the room temperature photoresponse of devices based on semimetal bismuth nanowire arrays capped by graphene. Our study was motivated by recent

reports of room temperature photodetectors based on bismuth. Here we demonstrate the optoelectronic properties of bismuth graphene interfaces. Our model of the bismuth graphene contact is similar to the one that is successfully employed for metal graphene except that we pointed out that the screening length Λ for Bi is much larger than for metals. The interfacial dipole is characterized via graphene Raman spectroscopy that allows measurement of the doping. The large doping that is observed is caused by the very low work function of Bi compared to graphene. Accordingly, zero-bias photocurrents are generated in an internal photoemision process at the interface between nanowire arrays and graphene where there is a large electrical dipole associated with the work functions. The large charge transfer for Bi nanowires in comparison to the Bi crystal sample is assigned to curvature induced electric field enhancements (lighting-rod effect). The thermoelectric signal cannot be observed. Intriguingly, the photoresponse exhibits a power-law frequency dependence over three order of magnitude of excitation frequency consistent with a wide distribution of diffusion times with an overall time of ~1 second. This characterization fits the model of Levy paths that explains anomalous transport in quantum-dot arrays. This is the first instance that fractional statistics have been proposed for photocurrent generation in graphene hybrids. Our results for the interface energies and doping compare fairly with DFT studies for Bi-adatoms on graphene.

ACKNOWLEDGEMENTS

This work was supported by the National Science Foundation through PREM 1205608 and STC CIQM 1231319. We also acknowledge support by The Boeing Company and The Keck Foundation.

REFERENCES

[1] A. K. Geim and K. S. Novoselov, The rise of graphene, Nat. Mater. 6, 183–191 (2007).

[2] K. I. Bolotin, K. Sikes, Z. Jiang, M. Klima, G. Fudenberg, J. Hone, P. Kim, H. Stormer, Ultrahigh electron mobility in suspended graphene, Solid State Commun. **146**, 351 (2008).

[3] G. Giovannetti, P. A. Khomyakov, G. Brocks, V. M. Karpan, J. van den Brink, and P. J. Kelly. Doping Graphene with Metal Contacts. Phys. Rev. Lett. 101, 026803 (2008).

[4]. A. Das, S. Pisana, B. Chakraborty, S. Piscanec, S. K. Saha, U. V. Waghmare, K.S. Novoselov, H. R. Krishnamurthy, A. K. Geim, A. C. Ferrari, and A. K Sood, Monitoring dopants by Raman scattering in an electrochemically top-gated graphene transistors, Nature Nanotech. **3**, 210 (2008).

[5] F. H. Koppens, T. Mueller, Ph. Avouris, A. Ferrari, M. Vitiello, M. Polini, Photodetectors based on graphene, other two-dimensional materials and hybrid systems, Nat. Nanotechnol. **9**, 780 (2014).

[6] T. Mueller, F. Xia, Ph. Avouris, Graphene photodetectors for high-speed optical communications, Nat. Photonics. **4**, 297 (2010).

[7] D. Spirito., et al. High performance bilayer-graphene terahertz detectors. Appl. Phys. Lett. **104**, 061111 (2014).

[8] L. Vicarelli, MS. Vitiello, D. Coquillat, A. Lombardo, AC. Ferrari, W. Knap, M. Polini, V. Pellegrini, A. Tredicucci. Graphene field-effect transistors as room-temperature terahertz detectors. Nat. Mater. **11**, 865 (2012).

[9] L. Viti, A. Politano, and M.S. Vitiello. Black phosphorus nanodevices at terahertz frequencies: Photodetectors and future challenges. Appl. Phys. Lett. Materials **5**, 035602 (2017).

[10] A. Politano., et al. The role of surface chemical reactivity in the stability of electronic nanodevices based on two-dimensional materials “beyond graphene” and topological insulators. FlatChem **1**, 60 (2017).

[11] A. Politano, L. Viti, and MS. Vitiello. Optoelectronic devices, plasmonics, and photonics with topological insulators. Appl. Phys. Lett. Materials **5**, 035504 (2017).

[12] L. Viti., et al. Black phosphorus terahertz photodetectors. Advanced Materials **27** 5567 (2015).

[13] A. Agarwal., et al. Plasmonics with two-dimensional semiconductors: from basic research to technological applications. Nanoscale **10,** 8938 (2018).

[14] T. J. Echtermeyer, P. S. Nene, M. Trushin, R. V. Gorbachev, A. L. Eiden, S. Milana, Z. Sun, J. Schliemann, E. Lidorikis, K. S. Novoselov, and A. C. Ferrari. Photothermoelectric and Photoelectric Contributions to Light Detection in Metal–Graphene–Metal Photodetectors. Nano Lett., 14, 3733 (2014).

[15] N. M. Gabor, J. C. W. Song, Q. Ma, N. L.Nair, T. Taychatanapat, K. Watanabe, T. Taniguchi, L. S. Levitov, P. Jarillo-Herrero. Hot Carrier Assisted Intrinsic Photoresponse in Graphene. Science 334, 648 (2011).

[16] J. Hicks, A. Tejeda, A. Taleb-Ibrahimi, M. Nevius, F. Wang, K. Shepperd, J. Palmer, F. Bertran, P. Le Fèvre, J. Kunc, W. de Heer, C. Berger and E. Conrad. A wide-bandgap metal–semiconductor–metal nanostructure made entirely from graphene, Nature Physics **9**, 49 (2013)**.**

[17] K. Roy, M. Padmanabhan, S. Goswami, T. Sai Phanindra, G. Ramalingam, S. Raghavan, A. Ghosh, Graphene–MoS2 hybrid structures for multifunctional photoresponsive memory devices, Nature Nanotechnol. **8**, 826 (2013).

[18] W. Zhang, C-P Chuu, J. K. Huang, C-H. Chen, M-L Tsai, Y-H Chang, C-T Liang, Y-Z Chen, Y-L Chueh, J-H. He, M-Y Chou, L-J. Li, Ultrahigh-gain photodetectors based on atomically thin graphene-MoS2 heterostructures, Sci. Rep. **4**, 3826 (2014).

[19] H. Qiao, J. Yuan, Z. Xu, C. Chen, S. Lin, Y. Wang, J. Song, Y. Liu, Q. Khan, H-Y. Hoh, C-X. Pan, S. Li, Q. Bao, Broadband photodetectors based on graphene–Bi_2Te_3 heterostructure, ACS Nano. **9**, 1886 (2015).

[20] C-C. Chen, M. Avkol, C-C Chang, A.F.J. Levi, S. B. Cronin. Graphene-silicon Schottky diodes, Nano Lett. **11**, 1863 (2011).

[21] L-H Zeng, M-Z Wang, H. Hu, B. Nie, Y-Q Yu, C-Y Wu, L. Wang, J-G. Hu, C. Xie, F-X Liang, and L-B. Luo. Monolayer graphene/germanium Schottky junction as high-performance self-driven infrared light photodetector, ACS Appl. Mater. Interfaces **5**, 9362 (2013).

[22] J.-P. Michenaud and J.-P. Issi, Electron and hole transport in bismuth, J. Phys. C 5, 3061 (1972).

[23] T. Huber, S. Johnson, L. Konopko, A. Nikolaeva, A. Kobylianskaya, M. J. Graf, Spiral modes and the observation of quantized conductance in the surface bands of bismuth nanowires, Sci. Rep. **7**, 15569 (2017).

[24]. F. Xia, T. Mueller, R Golizadeh-Mojarad, M. Freitag, Y-M Lin, J. Tsang V. V. Parebeinos, Ph. Avouris, Photocurrent imaging and efficient photon detection in a graphene transistor, Nano Lett. **9**, 1039 (2009).

[25]. F. Xia, V. Parebeinos, Y. M. Lin, Y. Wu, P. Avouris, Ultrafast graphene photodetector, Nature Nanotech. **6**, 179 (2009).

[26] A. Di Bartolomeo, Graphene Schottky diodes: An experimental review of the rectifying graphene/semiconductor heterojunctions, Phys. Rep. **606**, 1 (2016).

[27] I. K.Yanson and Y. G. Naidyuk. *Point-contact Spectroscopy*. (Springer, New York, 2005).

[28] W. Monch. On the physics of metal-semiconductor interfaces. Rep. Prog. Phys. **53**, 221-278 (1990).

[29]. S. M. Sze, *Physics of Semiconductor Devices* (John Wiley, New York, 1981), 2nd ed.

[30]. J. D. Yao, J. M. Shao, G. W. Yang, Ultra-broadband and high responsive photodetectors based on bismuth film at room temperature, Sci. Rep. **5**, 12320 (2015).

[31]. X. J. Yao, Z. Zheng, J. Shao, G. Yang. Promoting photosensitivity and detectivity of the Bi/Si heterojunction photodetector by Inserting a WS_2, ACS Appl. Mater. Interfaces **7**, 26701 (2015).

[32]. J. Reppert, R. Rao, M. Skove, J. He, M. Craps, T. Tritt, A. M. Rao. Laser-assisted synthesis and optical properties of bismuth nanorods, Chem. Phys. Lett. **442**, 334 (2007).

[33]. A. J. Levin, M. R. Black, M. S. Dresselhaus, Indirect L to T point optical transition in bismuth nanowires, Phys. Rev. **B79**, 165117 (2009).

[34]. T. W. Cornelius, M. E. Toimil-Molares, R. Neumann, G. Fahsold, R. Lovrincic, A. Pucci and S. Karim. Quantum size effects manifest in infrared spectra of single bismuth nanowires, Appl. Phys. Lett. **88**, 103114 (2006).

[35]. See Supplemental Material at [*URL will be inserted by publisher*] for a discussion of e-h pairs in bismuth, an overview of the fabrication of Bi nanowire arrays using the high pressure injection method and a table of the Raman peaks that were observed.

[36]. P. A. Khomyakov, G. Giovannetti, P. C. Rusu, G. Brocks, J. van den Brink and P. J. Kelly. First-principles study of the interaction and charge transfer between graphene and metals, Phys. Rev. B: Condens. Matter. Mater. Phys. **79**, 195425 (2009).

[37]. L. G. Cancado, A. Jorio, E. H. Martins Ferreira, F. Stavale, C. A. Achete, R. B. Capaz, M. V. O. Moutinho, A. Lombardo, T. S. Kulmala, and A. C. Ferrari, Quantifying defects in graphene via Raman spectroscopy at different excitation energies, Nano Lett. **11**, 3190 (2011).

[38]. M. S. Dresselhaus, A. Jorio, M. Hofmann and G. Dresselhaus and R. Saito, Perspectives on carbon nanotubes and graphene Raman spectroscopy, Nano Lett. **10**, 751 (2010).

[39]. R. Beams, L. G. Cancado, L. Novotny, Raman characterization of defects and dopants in graphene, J. Phys.: Condens. Matter. **27**, 083002 (2014).

[40]. X. Xu, N. Gabor, J. Alden, A. M. van der Zande, P. L. McEuen, Photo-thermoelectric effect at a graphene interface junction, Nano Lett. **10**, 562 (2011).

[41]. T. E. Huber, S. R. Johnson, T. Brower, J. H. Belk, J. H. Hunt, Photoresponse in arrays of thermoelectric nanowire junctions, Appl. Phys. Lett. **103**, 041114 (2013).

[42] Y. M. Zuev, W. Chang, and P. Kim. Thermoelectric and Magnetothermoelectric Transport Measurements of Graphene Phys. Rev. Lett. 102, 096807 (2009).

[43] J. Heremans, C. M. Thrush, Yu-Ming Lin, S. Cronin, Z. Zhang, M. S. Dresselhaus and J. F. Mansfield. Bismuth nanowire arrays: Synthesis and galvanomagnetic properties. Phys. Rev. B61, 2921 (2000).

[44]. T. E. Huber, K. Owusu, S. Johnson, A. Nikolaeva, L. Konopko, R. C. Johnson and M. J. Graf,

Surface State Band Mobility and Thermopower in Semiconducting Bismuth Nanowires, Phys. Rev. **B83**, 235414 (2011).

[45]. T. E. Huber, A. Nikolaeva, L. Konopko. M. J. Graf, Observation of three-dimensional behavior in surface states of bismuth nanowires and the evidence for bulk Bi charge fractionalization, Phys. Rev. **B79**, 201304 (2009).

[46]. G. Grzela, R. Paniagua-Domínguez, T. Barten, Y. Fontana, J. Sanchez-Gil, J. Rivas, Nanowire Antenna Emission, Nano Lett. **12**, 5481 (2012).

[47]. Z. Fan, R. Kapadia, P. Leu, X. Zhang, Y. Chueh, K. Takei, K. Yu, A. Jamshidi, A. Rathore, D. Ruebusch, M. Wu, A. Javey, Ordered arrays of dual-diameter nanopillars for maximized optical absorption, Nano Lett. **10**, 3823 (2010).

[48]. C. X. Lin and M. L. Povinelli, Optical absorption enhancement in silicon nanowire arrays with a large lattice constant for photovoltaic applications, Opt. Express 17, 19371 (2009).

[49]. D. Abujetas, R. Pangiangua-Dominguez, J. Sanchez-Gil. Unraveling the Janus Role of Mie resonances and leaky/guided models in semiconductor nanowire absorption for enhanced light harvesting, ACS Photonics **2**, 921 (2015).

[50]. K. Seo, M. Wober, P. Steinvurzel, E. Schonbrun, Y. P. Dan, T. Ellenbogen and K. B. Crozier, Multicolored Vertical Silicon Nanowires, Nano Lett. **11**, 1851 (2011).

[51]. M. Heiss, E. Russo-Averchi, A. Dalmau-Mallorqui, G. Tutuncuoglu, F. Matteini, D. Ruffer, S. Conesa-Boj, O. Demichel, E. Alarcon-Llado, A. F. Morral. III-V Nanowire Arrays: Growth and Light Interaction, Nanotechnology **25**, 014015 (2014).

[52]. K. T. Fountaine, W-H. Cheng, C. R. Bukowsky, H. A. Atwater. Near-unity unselective absorption in sparse InP nanowire arrays, ACS Photonics **3** 1826 (2016).

[53]. L. Xiaogang, P. R. Coxon, M. Peters, B. Hoex, J. M. Cole, D. J. Fray, Black Silicon: Fabrication Methods, Properties and Solar Energy Applications, Energy Environ. Sci. **7**, 3224 (2014).

[54]. E. Garnett, P. Yang. Light Trapping in Silicon Nanowire Solar Cells, Nano Lett. **10**, 1082 (2010).

[55]. J. Yao, Z. Liu, Y. Liu, Y. Wang, C. Sun, G. Bartal, A. Stacy, X. Zhang. Optical negative

refraction in bulk metamaterials of nanowires, Science **321**, 930 (2008).

[56]. K. Fountaine, W. Whitney, and H. A. Atwater, Resonant absorption in semiconductor nanowires and nanowire arrays: Relating leaky waveguide modes to Bloch photonic crystal modes, J. Appl. Phys. **116**, 153106 (2014).

[57]. G. Fan, H. Zhu, K. Wang, J. Wei, X. Li, Q. Shu, N. Guo, D. Wu, Graphene/Silicon Nanowire Schottky Junction for Enhanced Light Harvesting, ACS App. Mater. Interfaces. **3**, 721 (2011).

[58]. C. Xie, P. Lv, B. Nie, J. Jie, X. Zhang, P. Jiang, Z. Hu, L. Luo, Z. Zhu, Z. *et al*. , Monolayer graphene film/silicon nanowire array Schottky junction solar cells, Appl. Phys. Lett. **99**, 133113 (2011).

[59]. H. Park, S. Chang, J. Jean, J. J. Cheng, P. Araujo, M. Wang, M. Bawendi, M. S. Dresselhaus, V. Bulovic, J. Kong, *et al.* Graphene cathode-based ZnO nanowire hybrid solar cells, Nano Lett. **13**, 233 (2013).

[60]. X. Li, H. Zhu, K. Wang, A. Cao, J. Wei, C. Li, Y. Jia, Z. Li, X. Li, D. Wu, Graphene-on-silicon Schottky junction solar cells, Adv. Mater. **22**, 2743 (2010).

[61]. S. Tongay, M. Lemaitre, X. Miao, B. Gila, B. R. Appleton and A. F. Hebard, Rectification at graphene-semiconductor interfaces, Phys. Rev. X, **2**, 011002 (2012).

[62]. J. S. Lannin, J. M. Calleja and M. Cardona, Second-order Raman scattering in the group V_b semimetals: Bi, Sb, and As, Phys. Rev. **B12**, 585 (1975).

[63]. M. Muntwiler and X-Y Zhu, Image-potential states on the metallic (111) surface of bismuth, New J. Phys., **10**, 113018 (2008).

[64]. Y. J. Yu, Y. Zhao, S. Ryu, L. E. Brus, K. S. Kim, and P. Kim, Tuning the graphene work function by electric field, Nano Lett. **9,** 3430 (2009).

[65]. S. M. Song, S. J. Park, O. J. Sul, and B. J. Cho, Determination of work function of graphene under a metal electrode and its role in contact resistance, Nano Lett. **12,** 3887 (2012).

[66]. O. U. Akturk and M. Tomak, Bismuth doping of graphene, Appl. Phys. Lett. **96**, 081914 (2010).

[67]. H. H. Chen, S. H., S. L. Chang, B. Y. Cheng, S. W. Chen, H. Y. Chen, M. F. Lin, J. C. A Huang. Tailoring low-dimensional structures of bismuth on monolayer epitaxial graphene, Sci. Rep., **5**, 11623 (2005).

[68]. D. S. Nokidov, M. Drndic, L. S. Levitov, M. A Kasner, M. V. Jarosz, and M. G. Bawendi, Lévy statistics and anomalous transport in quantum-dot arrays, Phys. Rev. **B72**, 075309 (2005).

[69]. Y. M. Sheu, Y. J. Chien, C. Uher, S. Fahy and D. A. Reis, D. A. Free-carrier relaxation and lattice heating in photoexcited bismuth, Phys. Rev. **B87** 075429 (2013).

[70]. J-L. Ge, T-R. Wu, M. Gao, Z-B. Bai, L. Cao, X-F. Wang, Y-Y. Qin, F-Q. Song, Weak localization of bismuth cluster-decorated graphene and its spin interaction, Front. Phys. **12**, 127210 (2017).

[71]. L. Jin, L., L. Xiao, D. Zhang, H. Zhang, X. Tang, Z. Zhong and Q. Yang. Giant optical absorption and low dark current characteristics in wrinkled single layer graphene/bismuth nanorods, Carbon 127, 596 (2018).